A Dual-memory Permanent Magnet Brushless Machine for Automotive Integrated Starter-Generator Application

Wenlong Li, Christopher H.T. Lee, and Chunhua Liu
Department of Electrical and Electronic Engineering, The University of Hong Kong, Hong Kong
wlli@eee.hku.hk, *htlee@eee.hku.hk*, *chualiu@eee.hku.hk*

***Abstract*-This paper presents a dual-memory permanent magnet brushless machine for automotive integrated starter-generator (ISG) application. The key is that the proposed machine adopts two kinds of PM materials, namely NdFeB and AlNiCo for hybrid excitations. Due to the non-linear characteristic of demagnetization curve, AlNiCo can be regulated to operate at different magnetization levels via a magnetizing winding. With this distinct merit, AlNiCo can provide the assistance for online tuning the air-gap flux density. Firstly, the configuration of proposed machine is presented. Secondly, the finite element method (FEM) is applied for the field calculation and performance verification. Finally, both simulation and experimental results confirm that the proposed machine is very suitable for the ISG application.**

I. INTRODUCTION

The integrated starter-generator (ISG) combines the starter motor for internal combustion engine (ICE) cranking and the on-board alternator for electricity generation into a single device [1]. By this integration, the vehicle power train system can be downsized and the efficiency can be improved accordingly. Nowadays, hybrid electric vehicles (HEVs) are accepted as an optimum choice for solving the energy crisis and environment deterioration in the next decades. By using an ISG in the HEV, the fuel economy and efficiency can be further enhanced. In HEVs, the ISG not only provides starting torque for ICE and produces electricity for battery pack, but also can help to enhance the output torque of the ICE.

Due to its multiple utilizations, a good electric machine candidate for the ISG should meet some basic requirements: the high starting torque and the good capability for a wide constant-power speed range. A higher starting torque for cranking the engine to the idle speed, a shorter dynamic process can be obtained. Then from the speed above the idle speed to the maximum speed, the ISG works as an alternator for charging the battery pack. Because voltage rating of the power network in most of vehicles is 42 V, a high output voltage of the ISG may damage the vehicle, thus the ISG should have a good capability of flux weakening. Based on literature review, several types of electric machines, namely induction machine (IM), switched reluctance machine (SRM), and permanent magnet synchronous machine (PMSM) etc. are studied and applied for the ISG application [2]. The IM has a simple structure, low cost and mature control scheme, but for high speed operation, its power factor decrease dramatically. The SRM has a robust structure which is very suitable for high speed application, but it suffers from electric penalty, noise and low efficiency. Compared with the above two types, the PMSM possesses a lot of merits, such as high efficiency, high power density, and high starting torque etc. However, uncontrollable flux deteriorates its wide speed operation capability. The PMSM with interior or surface-inset PMs can solve this problem to some extent [3]-[6]. By controlling the direct-axis current to reduce the air-gap flux density, thus its constant-power speed range can be extended.

The purpose of this paper is to present a dual-memory permanent magnet brushless machine for ISG application, which also has salient structure but do not need to control direct-axis current for flux weakening. The key is that it adopts AlNiCo and NdFeB PMs for hybrid excitations. By tuning magnetization level of the AlNiCo PMs via a DC current pulse, the air-gap flux density can be controlled. Compared to those hybrid PM machines, it only needs current pulse but not a continuously-fed current to realize the flux control. Therefore, its efficiency can be further improved. With this capability, the starting torque can be strengthened for the starting mode. In the high-speed operation mode, the output voltage can be maintained without controlling the direct-axis current.

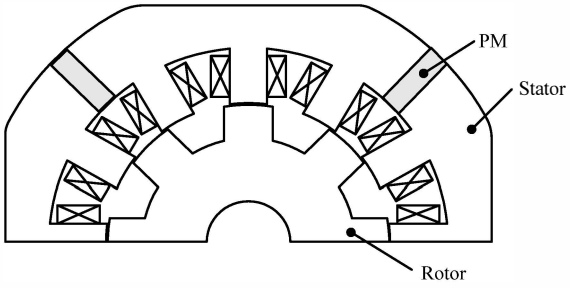

(a)

978-1-4673-2421-2/12/$31.00 ©2012 IEEE

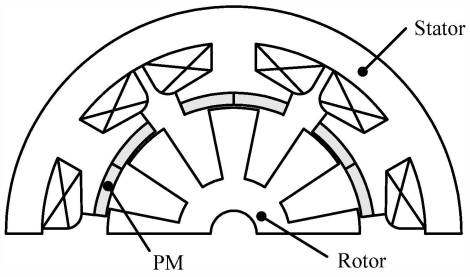

(b)

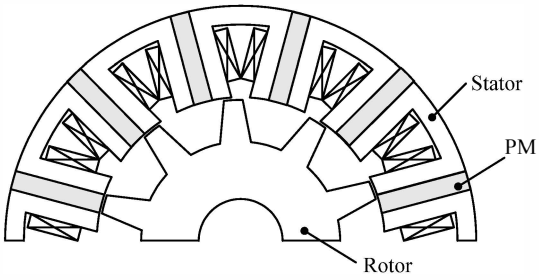

(c)

Fig. 1. Stator-PM machines. (a) DSPM. (b) FRPM. (c) FSPM.

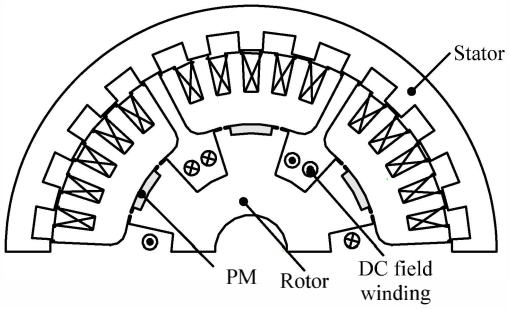

(a)

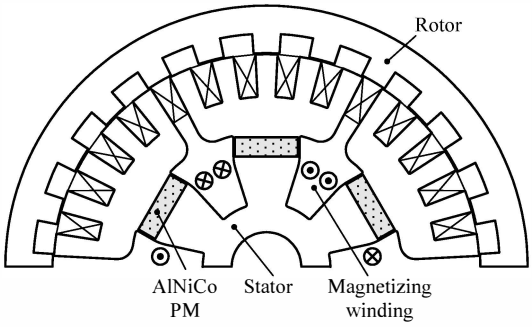

(b)

Fig. 2. Flux-controllable PM machines. (a) PMHB. (b) Memory machine.

II. MACHINE DESIGN

As stated before, the PM machines with saliency structure are more suitable for wide constant-power speed range applications due to the flux weakening capability. For high speed operation, the SRM is predominant due to its high robust, high reliable and low inertia characteristics. Thus, by combing the advantages of these two kinds of machines, the new machine is more favorable for the ISG application.

A. Stator-PM machines

As illustrated by the name, the stator-PM machines equip the PMs and armature windings in the stator [7]. The rotor consists of iron lamination only. Thus, the high-speed operation can be achieved without any accessories. According to the PM position in the stator, they can be categorized into three classes, namely doubly-silent PM (DSPM) machine [8]-[15], flux reversal PM (FRPM) machine [16]-[19] and flux switching PM (FSPM) machine [20]-[23]. As shown in Fig. 1, the DSPM machine has PMs in its back-iron. The flux variation in each winding is unipolar in the operation. The FRPM machine has PMs on surface of stator teeth. Each stator tooth has a pair of magnets of different polarity mounted at its surface. The flux variation in each winding is bipolar in the operation. The FSPM machine has PMs in the stator teeth, and the stator consists of U-shaped segments with PMs sandwiched between them. The flux variation in each winding is also bipolar in the operation. It should be emphasized that although these machine has a similar structure as SRM, the developed torque is mainly due to the electromagnetic torque but not the reluctance one. Although, they are suitable for high-speed operation, the flux control capability is not very strong. In order to enable the full flux control capability, flux controllable PM machine (FCPM) was proposed and it was also successfully applied in ISG for HEVs [24]. The flux control capability of FCPM machine is that using a direct-current (DC) field windings for assisting the air-gap flux control [25]-[28], as shown in Fig. 2(a). One drawback of this machine is that the DC field current should be continuously maintained for flux control, which inevitably incurs copper losses. In order to solve this problem, the novel FCPM machine called memory machine was proposed, as shown in Fig. 2(b). The memory machine adopts AlNiCo PMs for field excitation [29]-[34]. AlNiCo alloy has a non-linear relative permeability. By using a DC current pulse to magnetize or demagnetize AlNiCo, different magnetization levels can be memorized. Thus, different flux densities in the air-gap can be achieved.

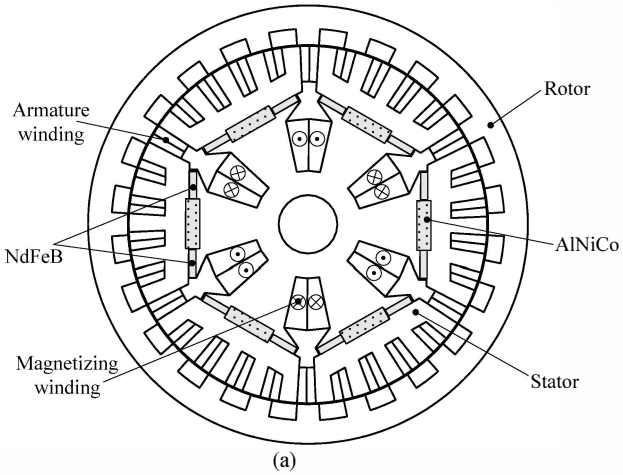

(a)

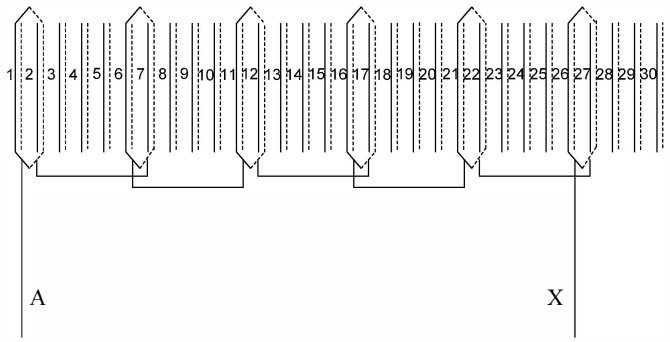

(b)

Fig. 3. Proposed machine. (a) Machine configuration. (b) Armature winding.

B. Proposed machine

The proposed machine is based on the aforementioned memory machine. Fig. 3(a) depicts the configuration of the proposed machine. The key of the proposed machine is to implement two kinds of PM materials for hybrid excitations. As shown in Fig. 3(a), the AlNiCo PMs are sandwiched by the NdFeB PMs. The NdFeB PMs provide the main air-gap flux, and the AlNiCo PMs assist the NdFeB PMs for regulating the air-gap flux density.

The proposed machine adopts an inner stator and outer rotor design. The armature windings are placed in the stator outer slot, the magnetizing windings are placed in the stator inner slot, and the PMs are placed between the two sets of windings. By placing the PMs in the back-iron, the PMs can avoid demagnetization by the armature reaction. This machine has 5 phases, and winding of phase A is shown in Fig. 3(b). The multi-phase design provides high fault tolerance capability. With even 2 phases are open circuited, the machine can still maintain an average output torque [35]. The magnetizing winding provides the magnetization or demagnetization of AlNiCo PMs. By applying a positive or negative DC current pulse to the magnetizing winding, the operating point of the AlNiCo PM is changed. After removing this DC pulse, the magnetization level of AlNiCo PM has been memorized. Thus, the air-gap flux density can be regulated.

TABLE I
KEY DESIGN DATA OF PROPOSED MACHINE

Rated power	1.2 kW
Rated torque	20 Nm
Speed range	0-4000rpm
No. of turns per armature coil	80
No. of turns per DC coil	420
Outer-rotor outside diameter	270.0 mm
Outer-rotor inside diameter	221.2 mm
Stator outside diameter	220.2 mm
Stack length	80.0 mm
AlNiCo PM dimensions (width × thickness)	33 × 8 mm
AlNiCo PM remanence and coercivity	1.3 T, 56 kA/m
NdFeB PM dimensions (width × thickness)	17.4 mm × 4 mm
NdFeB PM remanence and coercivity	1.3 T, 940 kA/m

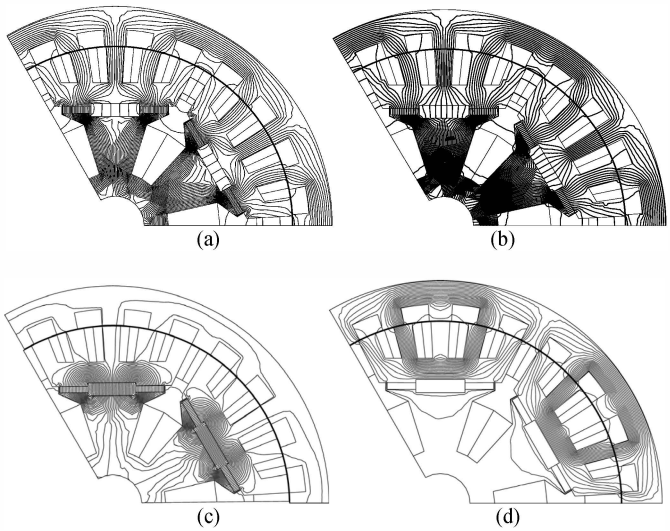

Fig. 4. Flux distributions. (a) NM-AlNiCo. (b) OM-AlNiCo. (c) IM-AlNiCo. (d) Armature reaction.

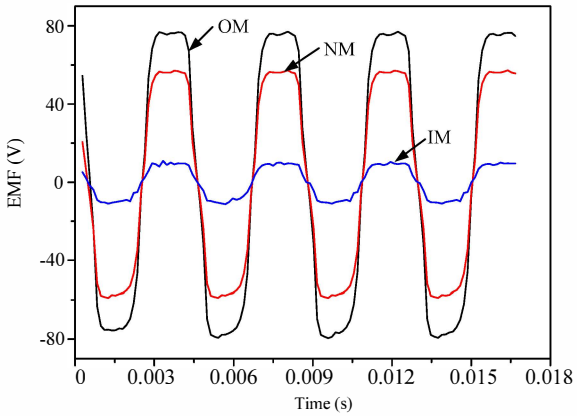

Fig. 5. Induced EMF under different magnetization.

III. MACHINE ANALYSIS

In order to access performances of the proposed ISG, the finite element method (FEM) is applied for the field calculation and performances verification. Due to the nonlinear characteristics of AlNiCo PMs, a parallelogram hysteresis model is adopted to fit its hysteresis loop which gives satisfactory results [36]. The key design data is listed in Table I.

Fig. 4 (a)-(c) shows the flux distributions of the proposed machine under different magnetization levels of AlNiCo PMs, namely non-magnetized (NM), outward-magnetized (OM) or flux strengthened, and inward-magnetized (IM) or flux weakened, respectively. It can be observed by OM, the flux lines are denser than the NM condition; by IM, the flux lines are sparser than the NM condition. It confirms the proposed machine has the capability for flux strengthening and weakening. Fig. 4(d) which illustrates the flux distribution due to armature excitation only shows that the armature reaction has limited influence on PMs. Most of the flux is shorted by the back-iron, which confirms that this

machine has a good immune to the armature reaction. After qualitatively studying its flux control capability, Fig. 5 quantitatively compares its flux regulation capability via the induced electromotive force (EMF) when the machine runs at 600 rpm under no-load condition. It can be seen that seen that the air-gap flux density can be controlled over 8 times between flux strengthening and weakening.

IV. CONTROL SCHEME

In order to evaluate the proposed machine for ISG operation, the dynamic and flux weakening control were carried out.

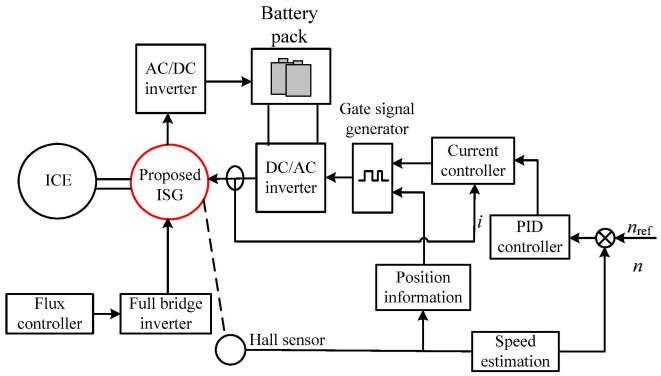

Fig. 6. Control block diagram.

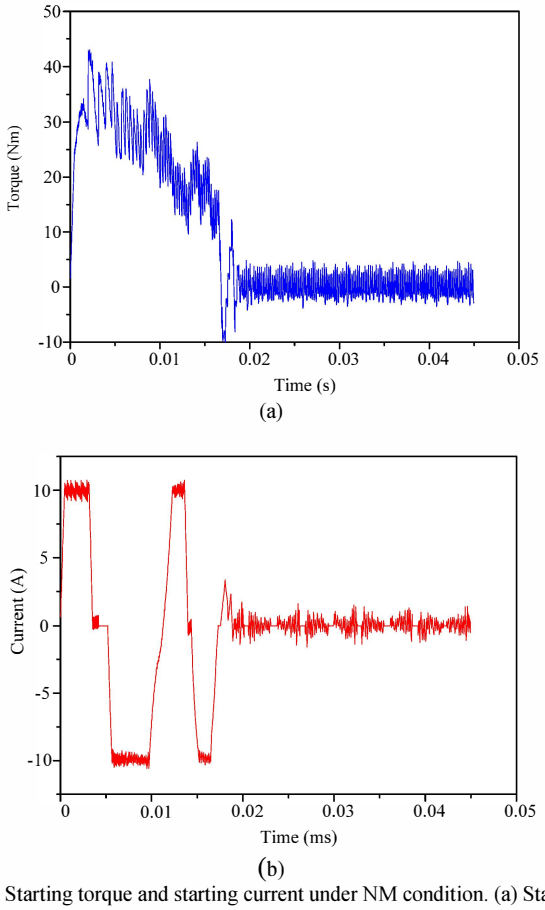

Fig. 7. Starting torque and starting current under NM condition. (a) Starting torque. (b) Armature current.

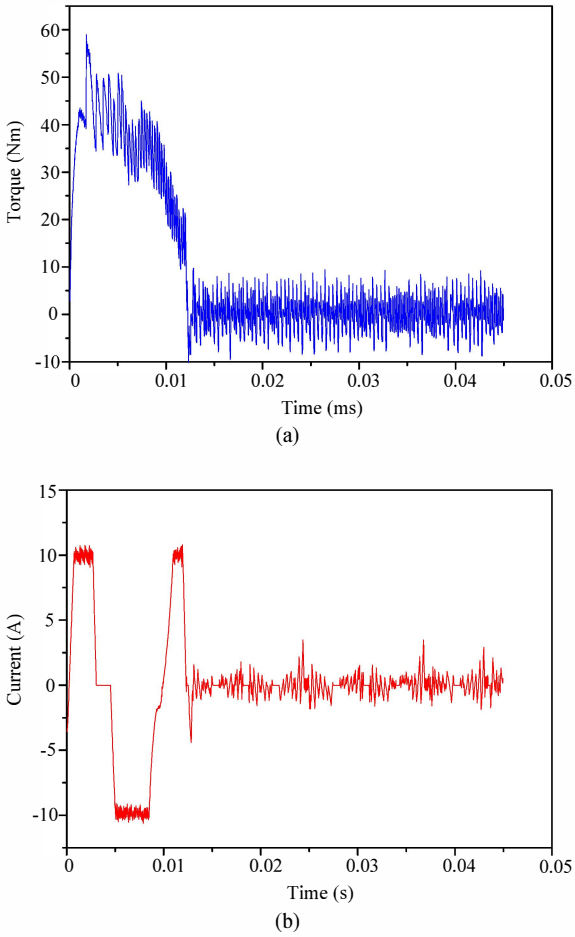

Fig. 8. Starting torque and starting current under OM condition. (a) Starting torque. (b) Armature current.

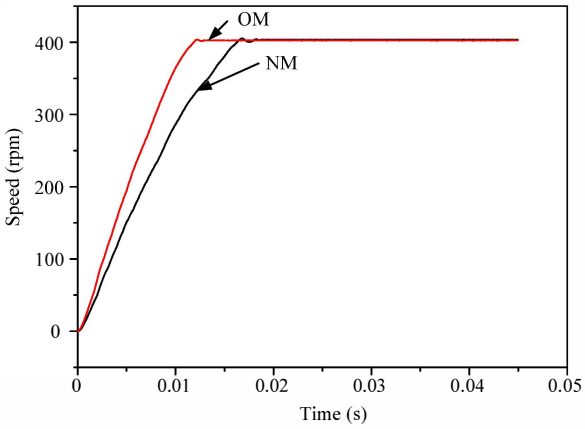

Fig. 9. Speed response characteristics.

Fig. 6 shows the control block diagram of the proposed machine for ISG operation. It consists of a dual-closed-loop control module and a flux control module. The dual-closed-loop control module is similar as that for the conventional permanent magnet brushless motor drives, namely a current loop and a speed loop. In the outer speed loop, the reference speed signal is compared with the feedback speed signal, and then the error information is input to the PID control unit to generate a current reference signal for the current control unit.

The signal from the current control unit along with the rotor position signal, are input to the 5-phase inverter to drive the motor. In the inner current loop control, the feedback current signal is compared with the current reference signal from the speed control unit, and then the error information is input to the current control unit to form the current loop control. The flux control unit serves as a stand-by unit to improve the ISG performance. In the engine cranking mode, a positive DC current pulse is applied to increase the air-gap flux density for strengthening the starting torque. For high-speed operation, a negative DC current pulse is applied to decrease the air-gap flux density. The DC current pulse is generated by a full bridge inverter. The amplitude of this current pulse is calculated from a look-up table.

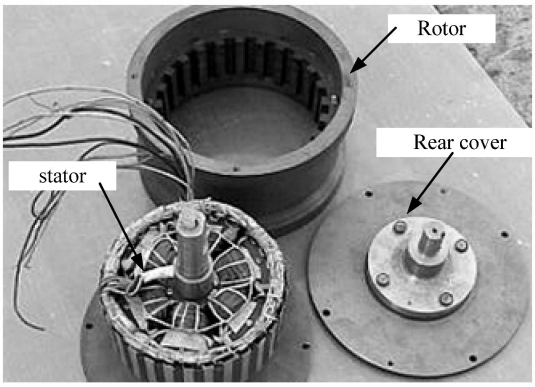

(a)

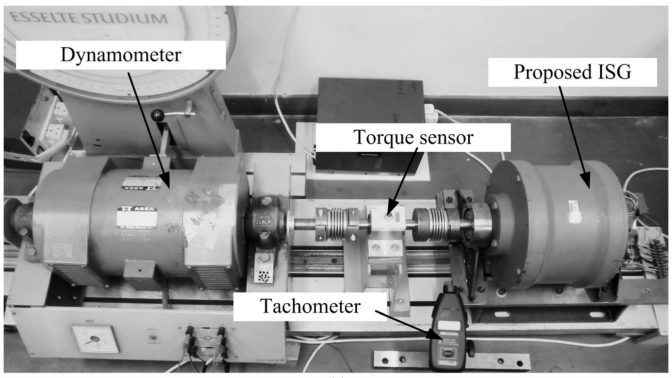

(b)

Fig. 10. Prototype. (a) Proposed machine. (b) Experimental set-up.

The engine cranking is the first important utilization of the ISG. When the automobile starts, the ISG needs to drive ICE to a base speed, which is called idle speed. In this stage, the AlNiCo should be fully strengthened for developing a high output torque. The flux control unit generates a positive DC current pulse to fully OM AlNiCo PMs. The idle speed of the engine is set as 400 rpm. Fig. 7 shows the starting torque and the armature current waveform when AlNiCo PMs are NM. It can be seen that a peak torque up to 42 Nm can be developed. The armature current is regulated by the current controller within 10 A. Fig. 8 shows the output torque and the armature current when AlNiCo PMs are fully OM. It can be observed that the output torque increases about 50% by strengthening the flux density, and the armature current are kept unchanged. Therefore, a shorter starting time can be achieved as shown in Fig. 9.

Electricity production is another important utilization of the ISG, since a lot of automobile consumer electronics are installed on board, the automobile electrification becomes a trend in recent several decades. In order to maintain a constant charging voltage, the flux should be weakened along with the engine speed. For verifying the flux weakening capability of the proposed machine, the experimentation is carried out. Fig. 10 shows the machine prototype and its test bed. As shown in the figure, a DC dynamometer is connected to the proposed machine via the same shaft. The DC dynamometer serves as a prime mover, while the proposed machine operates as a generator. The no-load electromotive force (EMF) waveforms under different speeds are measured. Fig. 11 (a) and (b) show the no-load EMF waveforms under different speeds without flux control. Fig. 11 (c) and (d) show the no-load EMF waveforms under the same speeds with flux control. Without flux control, the amplitude of no-load EMF depends on the rotor speed. A higher speed, a larger amplitude of EMF can be obtained. With flux control, the amplitudes of the EMF waveforms can be kept unchanged. It can be observed that with flux control the amplitude of EMF can be maintain at about 60 V. Therefore, the output voltage at rectifier terminal can be kept constant.

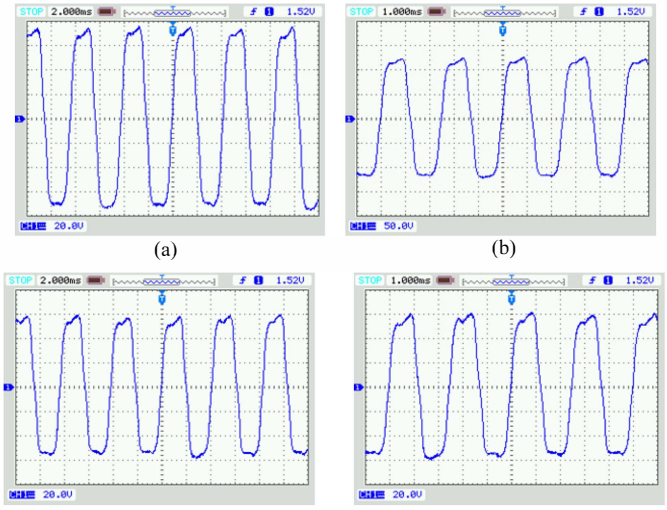

(a) (b) (c) (d)

Fig. 11. No-load EMF waveforms. (a) Without flux control at 600 rpm (20 V/div, 2ms/div). (b) Without flux control at 1000 rpm (50 V/div, 1ms/div). (c) With flux control at 600 rpm (20 V/div, 2ms/div). (d) With flux control at 1000 rpm (20 V/div, 1ms/div).

V. CONCLUSION

A dual-memory permanent magnet brushless machine for automotive ISG application is proposed and implemented in this paper. The key feature of the proposed machine is that it consists of AlNiCo and NdFeB PMs for hybrid excitations. The NdFeB PMs are engaged for providing main air-gap flux, while the AlNiCo PMs are used for regulating the flux

density via a temporary current pulse. Therefore, the proposed machine can achieve a high starting torque for engine cranking and wide constant-power speed range for electricity generation. Both the simulation and experimental results confirm that the proposed machine is very competent for ISG application.

ACKNOWLEDGMENT

This work was supported by a grant (Project No. HKU710710E) from the Hong Kong Research Grants Council, Hong Kong Special Administrative Region, China.

REFERENCES

[1] K.T. Chau and C.C. Chan, "Emerging energy-efficient technologies for hybrid electric vehicles," *Proceedings of IEEE*, vol. 95, no. 4, April 2007, pp. 821-835.

[2] G. Friedrich and A. Girardin, "Integrated starter generator," *IEEE Industry Applications Magazine*, vol. 15, No. 4, July-Aug. 2009, pp.26-34.

[3] L. Alberti, M. Barcaro, M.D. Pre, A. Faggion, L. Sgarbossa, N. Bianchi, S. Bolognani, "IPM machine drive design and tests for an integrated starter-alternator application," *IEEE Transactions on Industry Applications*, vol. 46, no. 3, May/June 2010, pp.903-1001.

[4] M.F. Rahman, L. Zhong, and W. L. Khiang, "A direct torque-controlled interior permanent magnet synchronous motor drive incorporating field weakening," *IEEE Transactions on Industry Applications*, vol. 34, no/ 6, Nov/Dec 1998, pp. 1246-1253.

[5] J. Gan, K.T. Chau, C.C. Chan and J.Z. Jiang, "A new surface-inset, permanent-magnet, brushless DC motor drive for electric vehicles," *IEEE Transactions on Magnetics*, vol. 36, no. 5, September 2000, pp. 3810-3818.

[6] Y. Wang, K.T. Chau, C.C. Chan and J.Z. Jiang, "Design and analysis of a new multiphase polygonal-winding permanent-magnet brushless dc machine," *IEEE Transactions on Magnetics*, vol. 38, no. 5, September 2002, pp. 3258-3260.

[7] C. Liu, K.T. Chau, J.Z. Jiang and S. Niu, "Comparison of stator-permanent-magnet brushless machines," *IEEE Transactions on Magnetics*, vol. 44, no. 11, November 2008, pp. 4405-4408.

[8] K.T. Chau, M. Cheng, and C.C. Chan, "Performance analysis of 8/6-pole doubly salient permanent magnet motor," *Electric Machines and Power Systems*, vol. 27, no. 10, October 1999, pp. 1055-1067.

[9] M. Cheng, K.T. Chau, C.C. Chan, and E. Zhou, "Performance analysis of split-winding doubly salient permanent magnet motor for wide speed operation," *Electric Machines and Power Systems*, vol. 28, no. 3, March 2000, pp. 277-288.

[10] M. Cheng, K.T. Chau, and C.C. Chan, "Design and analysis of a new doubly salient permanent magnet motor," *IEEE Transactions on Magnetics*, vol. 37, no. 4, July 2001, pp. 3012-3020.

[11] K.T. Chau, M. Cheng and C.C. Chan, "Nonlinear magnetic circuit analysis for a novel stator-doubly-fed doubly-salient machine," *IEEE Transactions on Magnetics*, vol. 38, no. 5, September 2002, pp. 2382-2384.

[12] M. Cheng, K.T. Chau and C.C. Chan, "New split-winding doubly salient permanent magnet motor drive," *IEEE Transactions on Aerospace and Electronic Systems*, vol. 39, no. 1, January 2003, pp. 202-210.

[13] K.T. Chau, Q. Sun, Y. Fan and M. Cheng, "Torque ripple minimization of doubly salient permanent magnet motors," *IEEE Transactions on Energy Conversion*, vol. 20, no. 2, June 2005, pp. 352-358.

[14] K.T. Chau, Y.B. Li, J.Z. Jiang and C. Liu, "Design and analysis of a stator-doubly-fed doubly-salient permanent-magnet machine for automotive engines," *IEEE Transactions on Magnetics*, vol. 42, no. 10, October 2006, pp. 3470-3472.

[15] Y. Fan and K.T. Chau, "Design, modeling, and analysis of a brushless doubly fed doubly salient machine for electric vehicles," *IEEE Transactions on Industry Applications*, vol. 44, no. 3, May-June 2008, pp. 727-734.

[16] S. Andersson, I. Boldea, and T.J.E. Miller, "The flux-reversal machine: a new brushless doubly-salient permanent-magnet machine," *IEEE Transactions on Industry Applications*, vol. 33, no. 4, Jul/Aug 1997, pp. 925-934.

[17] I. Boldea, J. Zhang, and S.A. Nasar, "Theoretical characterization of flux reversal machine in low-speed servo drives-the pole-PM configuration," *IEEE Transactions on Industry Applications*, vol. 38, no. 6, Nov/Dec 2002, pp. 1549-1557.

[18] C. Wang, S.A. Nasar, and I. Boldea, "Three-phase flux reversal machine (FRM)," *IEE Proceedings –Electric Power Applications*, vol. 146, no. 2, March 1999, pp. 139-146.

[19] T. H. Kim, K. B. Jang, Y.D. Chun, and J. Lee, "Comparison of the characteristics of a flux reversal machine under the different dtiving methods," *IEEE Transactions on Magnetics*, vol. 41, no. 5, May 2005, pp. 1916-1919.

[20] Z.Q. Zhu, Y. Pang, D. Howe, S. Iwasaki, R. Deodhar, and A. Pride, "Analysis of electromagnetic performance of flux-switching permanent-magnet machines by nonlinear adaptive lumped parameter magnetic circuit model," *IEEE Transactions on Magnetics*, vol. 41, no. 11, November 2005, pp. 4277-4287.

[21] W. Hua, M. Cheng, Z. Q. Zhu, and D. Howe, "Analysis and optimization of back-emf waveform of a novel flux-switching permanent magnet motor," *IEEE Transactions on Energy Conversion*, vol. 23, no. 3, September 2008, pp.727-733.

[22] J.F. Bangura, "Design of high-power density and relatively high-efficiency flux-switching motor," *IEEE Transactions on Energy Conversion*, vol. 21, no. 2, June 2006, pp. 416-425.

[23] W. Zhao, M. Cheng, K.T. Chau, W. Hua, H. Jia, J. Ji, and W. Li, "Stator-flux-oriented fault-tolerant control of flux-switching permanent- magnet motor," *IEEE Transactions on Magnetics*, vol. 47, no. 10, October 2011, pp.4191-4194.

[24] C. Liu, K.T. Chau, and J.Z. Jiang, "A permanent-magnet hybrid brushless integrated- starter-generator for hybrid electric vehicles," *IEEE Transactions on Industrial Electronics*, vol. 57, no. 12, December 2010, pp. 4055-4064.

[25] C. Liu, K.T. Chau, J.Z. Jiang and L. Jian, "Design of a new outer-rotor permanent magnet hybrid machine for wind power generation," *IEEE Transactions on Magnetics*, vol. 44, no. 6, June 2008, pp. 1494-1497.

[26] C. Liu, K.T. Chau and W. Li, "Comparison of fault-tolerant operations for permanent-magnet hybrid brushless motor drive," *IEEE Transactions on Magnetics*, vol. 45, no. 6, June 2010, pp. 1378-1381.

[27] X. Zhu, K.T. Chau, M. Cheng and C. Yu, "Design and control of a flux-controllable stator-permanent magnet brushless motor drive," *Journal of Applied Physics*, vol. 103, no. 7, April 2008, paper no. 7F134, pp. 1-3.

[28] X. Zhu, M. Cheng, K.T. Chau, and C. Yu, "Torque ripple minimization of flux-controllable stator-permanent magnet brushless motors using harmonic current injection," *Journal of Applied Physics*, February 2009, 105(7): 07F102: 1-3

[29] V. Ostovic, "Memory motors," *IEEE Industry Applications Magazine*, vol. 9, no. 1, Jan/Feb 2003, pp. 52-61.

[30] V. Ostovic, "Pole-changing permanent-magnet machines," *IEEE Transactions on Industry Applications*, vol. 38, no. 6, Nov/Dec 2002, pp. 1493-1499.

[31] Y. Gong, K.T. Chau, J.Z. Jiang, C. Yu and W. Li, "Analysis of doubly salient memory motors using Preisach theory," *IEEE Transactions on Magnetics*, vol. 45, no. 10, October 2009, pp. 4676-4679.

[32] C. Yu, K.T. Chau, X. Liu and J.Z. Jiang, "A flux-mnemonic permanent magnet brushless motor for electric vehicles," *Journal of Applied Physics*, vol. 103, no. 7, April 2008, paper no. 07F103, pp. 1-3.

[33] C. Yu and K.T. Chau, "Dual-mode operation of DC-excited memory motors under flux regulation," *IEEE Transactions on Industry Applications*, vol. 47, no. 5, Sept.-Oct. 2011, pp. 2031-2041.

[34] C. Yu and K. T. Chau, "Design, analysis, and control of DC-Excited memory motors," *IEEE Transactions on Energy Conversion*, vol. 26, no. 2, June 2011, pp. 479-489.

[35] C. Yu and K.T. Chau, "A new fault-tolerant flux-mnemonic doubly-salient permanent-magnet motor drive," *IET Electric Power Applications*, vol. 5, no. 5, May 2011, pp. 393-403.

[36] W. Li, K.T. Chau, Y. Gong, J.Z. Jiang, and F. Li, "Design and analysis of a flux-mnemonic dual-magnet brushless machine," *IEEE Transactions on Magnetics*, vol.47, no. 10, pp.4223-4226.